

Functionalization of Graphene Oxide by Tetrazine Derivatives: A Versatile Approach toward Covalent Bridges between Graphene Sheets

Yuan Li,[†] Valérie Alain-Rizzo,[†] Laurent Galmiche,[†] Pierre Audebert,[†] Fabien Miomandre,^{*,†} Guy Louarn,[‡] Michael Bozlar,[§] Michael A. Pope,^{§,||} Daniel M. Dabbs,[§] and Ilhan A. Aksay^{*,§}

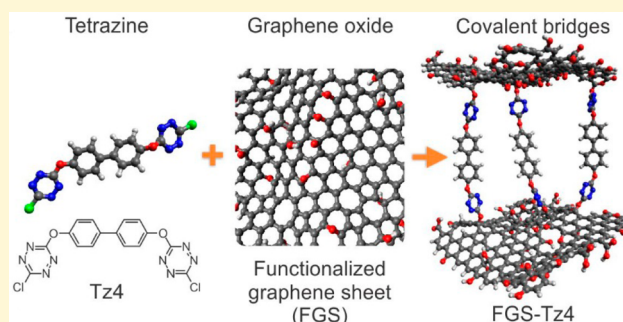
[†]PPSM, CNRS UMR8531, Ecole Normale Supérieure de Cachan, 61 Avenue Président Wilson, 94235 Cachan, France

[‡]Institut des Matériaux Jean Rouxel, Université de Nantes, CNRS, 2 rue de la Houssinière, 44322 Nantes, France

[§]Department of Chemical and Biological Engineering, Princeton University, Princeton, New Jersey 08544, United States

Supporting Information

ABSTRACT: We have covalently grafted tetrazine derivatives to graphene oxide through nucleophilic substitution. Since the tetrazine unit is electroactive and nitrogen-rich, with a reduction potential sensitive to the type of substituent and degree of substitution, we used electrochemistry and X-ray photoelectron spectroscopy to demonstrate clear evidence for grafting through covalent bonding. Chemical modification was supported by Fourier transform infrared spectroscopy and thermal analysis. Tetrazines grafted onto graphene oxide displayed different mass losses compared to unmodified graphene and were more stable than the molecular precursors. Finally, a bridging tetrazine derivative was grafted between sheets of graphene oxide to demonstrate that the separation distance between sheets can be maintained while designing new graphene-based materials, including chemically bound, redox structures.



INTRODUCTION

Graphene- and graphene-oxide-based nanomaterials have significant interest within the scientific community due to their outstanding mechanical and electrical properties, as well as their utility in myriad applications ranging from batteries,¹ solar cells,² transistors,³ and composite materials⁴ to medicine.⁵ Unlike pristine graphene, graphene oxide is an electrical insulator with a typical carbon-to-oxygen ratio (C/O) of ~ 2 .^{6,7} When partially reduced to an electrically conducting state,⁷ the C/O can range from ~ 6 to as high as 500. Due to the defective and functionalized structure of reduced graphene oxide, it has a more important role in applications where pristine graphene has limited utility.⁸ In order to differentiate between graphene oxides with different degrees of reduction, we refer to them as functionalized graphene sheets (FGSs) and designate the C/O value with a subscript after FGS. Thus, FGS₂ designates graphene oxide with a nominal C/O ~ 2 while FGS₂₀ refers to the material we obtain after the rapid thermal exfoliation of graphite oxide (GO), with a nominal C/O ~ 20 . FGS₂ is composed of sp^3 carbon atoms arranged in a two-dimensional hexagonal array with a variety of oxygen-containing functionalities on both sides of the array: primarily epoxy and hydroxyl groups on the basal plane and carboxylic acid, esters, phenols, and quinones at the sheet edges.⁹ The high number of oxygen functionalities on FGS₂ favors its

dispersion in polar solvents and provides convenient sites for further chemical functionalization through covalent bonding.

One of the main challenges in using graphene sheets in various applications is keeping the graphene sheets well-separated and avoiding aggregation induced by van der Waals interactions, while keeping the sheets linked together through a controlled mechanism.^{8,10} An ideal scenario to achieve this goal would be to covalently link adjacent sheets by short, rigid, and electrically conducting bridges. This would allow an FGS film's accessible surface area to be tailored without significantly disrupting its electrical conductivity. Commensurate with this goal, attaching organic molecules to FGS₂ and reduced graphene oxides (FGS_x with $x > 6$) has been reported in the literature, principally using the amide or ester groups as the links to the FGSs^{11,12} or by linking directly to the conjugated network using diazonium chemistry.^{13,14} Covalent links to FGS₂ have been claimed for a variety of molecules, including aromatic dyes like porphyrins,^{15,16} macrocycles like cyclodextrins,¹⁷ diaminoalkanes,¹⁸ azido-terminated poly(ϵ -caprolactone),¹⁹ and 4-*ter*-butylphenyl, the last using diazonium salts as linking agents.²⁰ In these compounds, covalent bonding is typically inferred using a combination of analytical techniques

Received: February 20, 2015

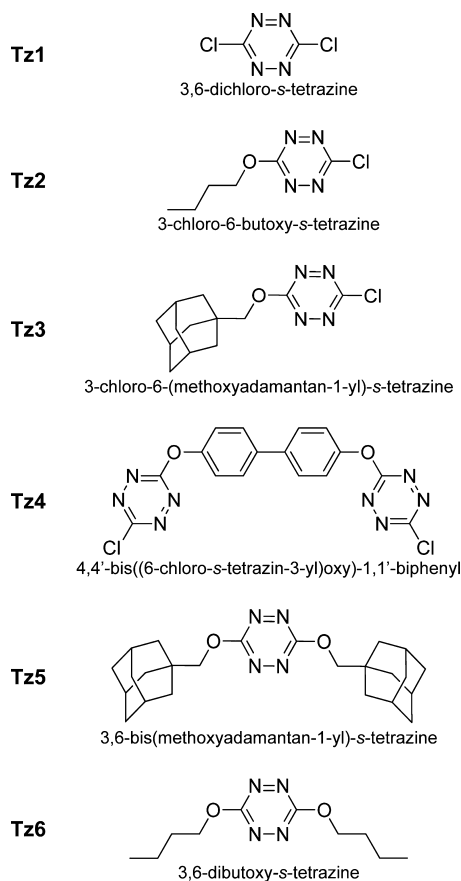
Revised: May 27, 2015

Published: May 28, 2015

such as Fourier transform infrared (FTIR) spectroscopy, ultraviolet and visible (UV/vis) spectroscopy, X-ray photoelectron spectroscopy (XPS), nuclear magnetic resonance (NMR) spectroscopy, and thermal analysis (TA).

In this paper, we describe a one-step covalent functionalization method to covalently bind substituted *s*-tetrazines to FGS₂ by a nucleophilic aromatic substitution reaction. The *s*-tetrazine moiety is a six member aromatic ring containing four nitrogen atoms in the 1, 2, 4, and 5 positions and two carbon atoms in the 3 and 6 positions of the ring, the latter providing sites for substituents.²¹ Using chlorine as a leaving group allows easy substitution by alkoxy groups in the presence of an appropriate non-nucleophilic base catalyst such as 2,4,6-trimethylpyridine (collidine) to create the monosubstituted tetrazines described in this paper. Thus, starting from 3,6-dichloro-*s*-tetrazine (Tz1), nucleophilic substitution allows the synthesis of 3-chloro-6-butoxy-*s*-tetrazine (Tz2), 3-chloro-6-(methoxyadamantan-1-yl)-*s*-tetrazine (Tz3), and the bridged 4,4'-bis((6-chloro-*s*-tetrazin-3-yl)oxy)-1,1'-biphenyl (Tz4) (Scheme 1).²² The 3,6-bis-

Scheme 1. Formulae and Names of the Various Substituted Tetrazines Used in This Study



(methoxyadamantan-1-yl)-*s*-tetrazine (Tz5) has a much lower vapor pressure than the other substituted tetrazines and was synthesized to aid in assigning the XPS features observed for a molecular tetrazine compound because the other tetrazines rapidly sublime under high vacuum. Tetrazine derivatives are versatile compounds that have the potential to react either by nucleophilic substitution at the hydroxyl groups present on FGS₂ or through inverse demand Diels–Alder reaction at the more extensive aromatic domains of highly reduced FGS₂ or

pristine graphene.²³ Besides these advantages in terms of material synthesis, tetrazines are also electroactive moieties enabling electrochemical characterization of the product and, in contrast to other analytical methods, provide direct evidence for covalent bonding.

The general procedures used to first synthesize and then graft the substituted chlorotetrazines onto FGS₂ are shown in Scheme 2. Tz1 is a versatile precursor for preparing a wide variety of substituted tetrazines through the displacement of a chlorine atom by a nucleophile such as an alcohol, thiol, or amine.²¹ Monosubstitution readily proceeds at room temperature, with yields of up to 90% of the theoretical yield based on the stoichiometry of the reaction shown in Scheme 2.²¹

Examples of materials to which tetrazines are claimed to be covalently attached include silica nanoparticles^{24,25} and carbon nanotubes,²⁶ but, to the best of our knowledge, this is the first study that clearly demonstrates the covalent functionalization of graphene oxide. The use of tetrazines for covalent modification of graphene oxide sheets opens the way toward bridging sheets with redox active structures, with the hope to drastically change the material properties and, among others, its ability to store charges.

RESULTS AND DISCUSSION

We characterized various tetrazine-functionalized FGSs (prepared as described in Methods and Materials) using electrochemistry, XPS, TA, and FTIR spectroscopy, to demonstrate that covalent links exist between the FGSs and the substituted tetrazines. GO is readily exfoliated in propylene carbonate (PC) to form dispersions of FGS₂,²⁷ facilitating the reaction between the FGS₂ and monosubstituted tetrazines (Scheme 2). The different FGS-Tz compounds remain dispersed in PC, and the highly colored tetrazine substituents are revealed by changes in the color and opacity of the suspension (Figure 1); however, this is an insufficient demonstration that the tetrazines are covalently grafted onto the FGSs. Thus, we used cyclic voltammetry, XPS, TA, and FTIR to determine if covalent grafting by the tetrazines does occur. Cyclic voltammetry reveals shifts in the redox potentials of the tetrazine as a result of replacing chlorine atoms with oxygen linkages to the graphene sheets. XPS measurements reveal changes in the ratio of carbon hybridization in the FGS and the presence of an oxygen atom shared between the tetrazine ring and the FGS as well as the presence of a significant amount of nitrogen in the final material. X-ray diffraction (XRD) shows structural modifications associated with the covalent grafting by the bridging tetrazine unit. TA confirms the amount of tetrazine grafted on the FGS indicated by XPS. FTIR reveals that a close association exists between the tetrazine and the FGS that cannot be removed by washing with solvent. These results are discussed in more detail in the following sections.

Electrochemistry. To illustrate the effect of alkoxy substitution on the electrochemistry of substituted tetrazine derivatives in solution, we show the cyclic voltammograms (CVs) of various tetrazines (Tz1, Tz2, Tz4, and Tz6), unmodified FGS₂, and the grafted FGS-Tz compounds in Figure 2. A gradual and significant shift in the reduction potential to more negative values is clearly observed as each chlorine atom is successively replaced by an alkoxy group, an effect demonstrated using mono- and disubstituted tetrazines (Figure 2a). The sequential shift is a result of the less electron withdrawing effect of the -OR group relative to that of a chlorine atom.²² In Figure 2b–d, we display the CVs of

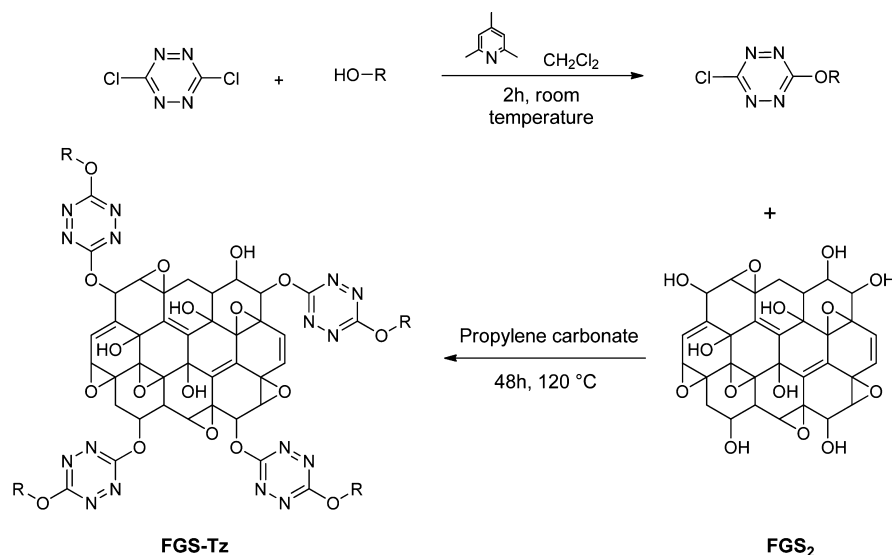
Scheme 2. General Synthetic Route Leading to the Grafting of Substituted Chlorotetrazines to FGS₂

Figure 1. Pictures of $0.3 \text{ g}\cdot\text{L}^{-1}$ suspensions of unmodified FGS₂ (left) and grafted FGS-Tz4 (right) in PC.

suspensions of various FGS-Tz compounds after redispersing the material in PC-based electrolyte using ultrasonication. For comparison, the CVs of the tetrazine precursors Tz1, Tz2, Tz4, and the unmodified FGS₂ measured under the same experimental conditions are superimposed on that of the related FGS-Tz compound.

In the case of Tz1, we observe only a broad signal, similar to the response of the unmodified FGS₂ (Figure 2b). If nucleophilic substitution was successful, we would expect to observe a reduction peak as the tetrazine moiety should remain electrochemically active. As discussed below, the attempted reaction between Tz1 and FGS₂ was unsuccessful. An obvious color change occurred upon mixing FGS₂, Tz1, and the catalyst in PC, without heating the mixture, suggesting that an undesirable side reaction occurred between the Tz1 and the other components of the suspension. The consumption of Tz1 was confirmed by the observation that no Tz1 could be recovered from the mixture via thin layer chromatography (TLC), used to detect the presence of any free tetrazine following reaction. The loss of Tz1 appears to have prevented any significant grafting onto the FGS₂. In contrast, the CVs recorded after reactions involving the other tetrazines (Tz2,

Tz3, and Tz4) and FGS₂ displayed a significant reduction peak, as illustrated in Figure 2c,d and Supporting Information Figure SI-1, strongly suggesting that grafting of the tetrazine onto the FGS was achieved in these compounds.

The new reduction peak features a significant negative shift in the reduction potential, relative to the peaks observed for the tetrazine precursor used in the grafting reaction (Figure 2c,d and Supporting Information Figure SI-1). No peaks remain that may be commensurate with what would be expected if an electron withdrawing chlorine on the precursor tetrazine was not replaced by an oxygen link to the FGS. The potential differences observed between the two curves are, respectively, 0.5, 0.6, and 0.8 V for FGS-Tz2, FGS-Tz3, and FGS-Tz4. This clearly indicates that the precursor reacted and, in addition, was no longer present in the final material as a discrete compound (indicating that none of the tetrazine remained physisorbed to the FGS).

As expected, the reduction of the tetrazine core in all FGS-Tz compounds is noticeably more difficult (i.e., occurs at lower reduction potentials) than in the precursor tetrazine. We attribute this to the substitution reaction that replaced the electron withdrawing chlorine atom by a more electron donating alkoxy group provided by the hydroxyl groups on the FGS₂. The same trend is observed with all compounds, except for Tz1, as illustrated in Figure 2 and in the Supporting Information (Figure SI-1). Moreover, the CVs of the FGS-Tz compounds combine the features of the unmodified FGS₂ with the corresponding dialkoxy-tetrazine, as shown in Figure 2c which compares the CVs of the unmodified FGS₂ with that of the disubstituted Tz6. From an electrochemical point of view, the electronic environment of the tetrazine core in Tz6 is similar to the one in FGS-Tz2 (with two alkoxy groups on the tetrazine core) and has a very different CV from that of the monosubstituted precursor Tz2. The CVs in Figure 2c exactly reflect the same similarity and difference when the peak positions are compared. Thus, the CVs offer clear evidence that covalent linkage between tetrazine and oxidized graphene through substitution of chlorine by oxygen has been achieved.

Moreover, a more negative shift is observed when a rigid bridging tetrazine (FGS-Tz4, Figure 2d) is used instead of a nonbridging tetrazine (FGS-Tz2 or FGS-Tz3). Since the

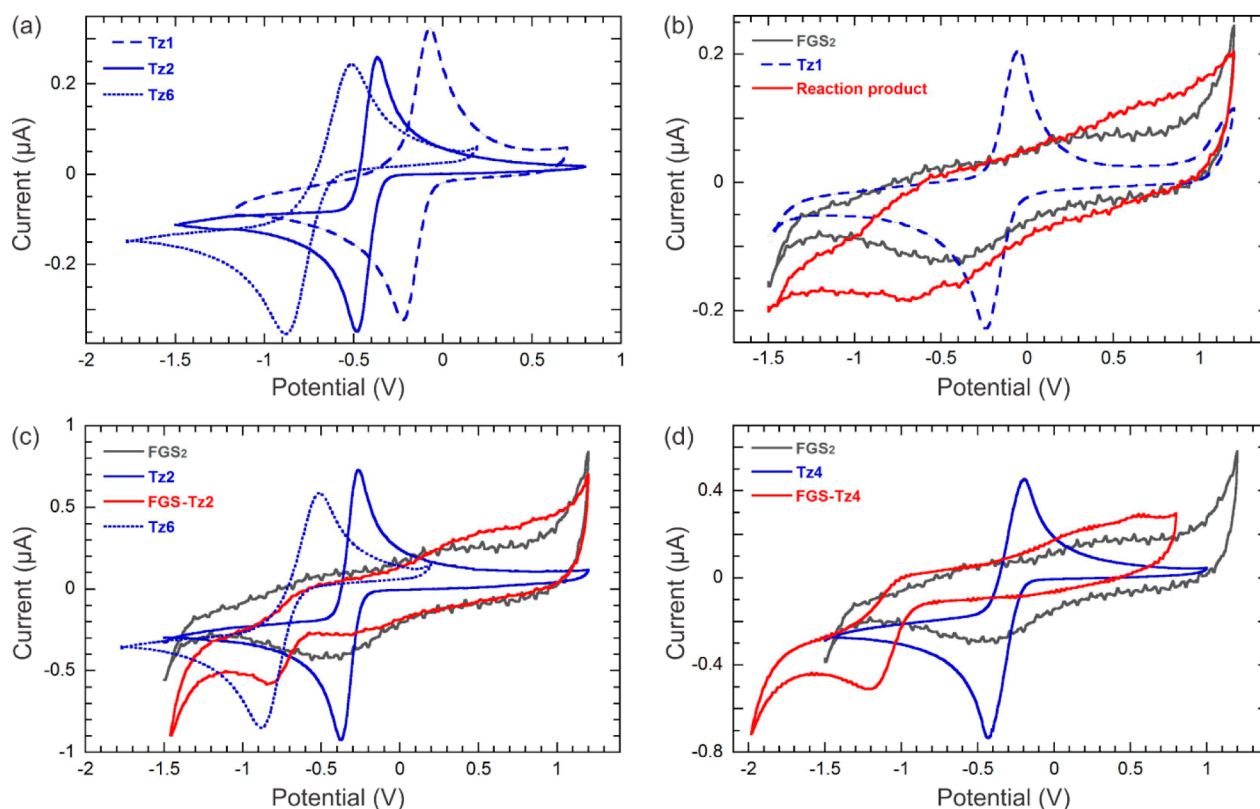


Figure 2. (a) CVs of 3,6-dichloro-*s*-tetrazine (Tz1) (blue dashed line), 3-chloro-6-butoxy-*s*-tetrazine (Tz2) (blue solid line), and 3,6-dibutoxy-*s*-tetrazine (Tz6) (blue dotted line). (b) CVs of Tz1 (blue dashed line), unmodified FGS₂ (gray), and the solid component of the product from the attempted reaction between Tz1 and FGS₂ (red). For the latter, there is no evidence that Tz1 is present, and the resulting CV resembles that of the unmodified FGS₂. (c) CVs of Tz2 (solid blue line), unmodified FGS₂ (gray), grafted FGS-Tz2 (red), and Tz6 (blue dashed line). (d) CVs of 4,4'-bis((6-chloro-*s*-tetrazin-3-yl)oxy)-1,1'-biphenyl (Tz4) (solid blue line), unmodified FGS₂ (gray), and grafted FGS-Tz4 (red). Each CV was made using suspensions (for FGS-Tz, ca. 0.5 mg/mL) or solutions (for Tz, ca. 0.5 mM) in propylene carbonate (with 0.1 M TBAPF₆ as the electrolyte) against a platinum electrode.

reduction potential is almost the same for the various precursor tetrazines possessing a chlorine substituent, this more negative potential shift in FGS-Tz4 supports the hypothesis that Tz4 forms a cross-link between separate FGS₂, introducing additional stress on the central link in the final material. In addition, no detectable electrochemical response was observed that could be assigned to the remaining chloro-alkoxy-tetrazine in this compound. This is an additional proof that not only does the bifunctional tetrazine react but that it appears to react *quantitatively at both ends*, therefore acting as a cross-linker in the compound, in addition to the incorporation of the tetrazine moieties.

We note, however, that a partial loss in reversibility in the backward scan for the tetrazine signals in all FGS-Tz compounds is observed, which is not fully understood at this point. This phenomenon is not observed in the tetrazine molecular compounds, unless protonation of the anion radical occurs at the end of the forward scan.^{21,28} A possible explanation might be that protonation occurs in graphene materials to some extent, because of the possible presence of neighboring carboxylic acid groups, which have been recognized in FGS₂,²⁹ especially in a moderately basic solvent like PC which is likely to assist the proton transfer.²⁷

X-ray Photoelectron Spectroscopy. The XPS spectra of the unmodified FGS₂ and grafted FGS-Tz compounds are shown in Figures 3–7. The elemental composition of the FGS₂ used in this study (Figure 3a) has a C/O close to 2.2 (± 0.1)

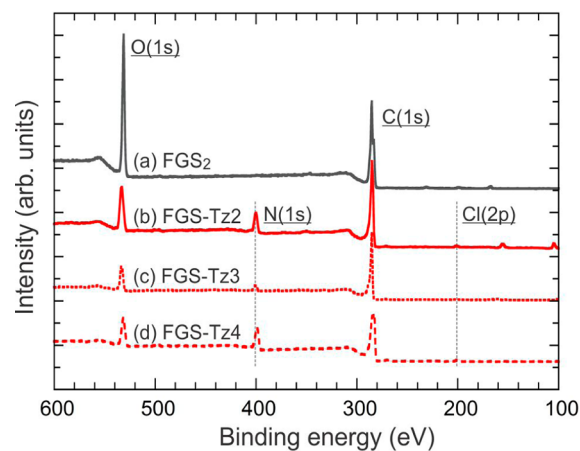


Figure 3. XPS spectra of (a) unmodified FGS₂, (b) FGS-Tz2, (c) FGS-Tz3, and (d) FGS-Tz4.

with only residual chlorine among other detected elements (Table 1). After grafting by tetrazine derivatives, the most striking feature in the XPS spectra of FGS-Tz compounds is the appearance of a new signal corresponding to N(1s) near 400 eV (Figure 3b,c,d). Also worth mentioning is the increase in the amount of carbon and the decrease in the oxygen content (Figure 3, Table 1) associated with the addition of the tetrazine moiety to the FGS. A slightly larger amount of chlorine Cl(2p) ($\cong 0.8 \pm 0.2\%$) is visible in FGS-Tz4, possibly indicating that a

Table 1. Atomic Percentages in unmodified FGS₂, Tz5, and FGS-Tz Compounds as Determined by XPS

	FGS ₂	FGS-Tz2	FGS-Tz3	FGS-Tz4	Tz5
%C	67.5	71.0	79.8	70.2	80.7
%N	0.0	12.1	5.8	18.0	12.4
%O	31.8	16.4	13.9	10.7	6.8
%Cl	0.28	0.50	0.37	0.8	0.0

small amount of the *bis*-tetrazine only reacted at one end, leaving one chlorine on the unbound end of the molecule. These features are consistent with a highly energetic interaction between graphene oxide and tetrazine, in which the chlorine atoms in the tetrazine precursors have been replaced by oxygens in the FGS₂-Tz.

When comparing the details of the different elemental signals in the unmodified FGS₂ (Figure 4), FGS-Tz (Figures 5 and 6), and the Tz5 compound (Figure 7), we note that in the unmodified FGS₂ (i) the C(1s) signal can be decomposed into three main contributions (Figure 4a), underlining the presence of at least 6 types of carbon bonds: *sp*² aromatic and *sp*³ carbons (284.5 eV), C—O—C epoxy ring, and C—OH (286.5 eV), C=O and O—C=O (288.2 eV), while (ii) the O(1s) signal contains a main signal centered at 532.3 eV and divided into two contributions (see the assignment in Figure 4b).^{30–32} After chemical grafting, in the FGS-Tzs the C—C (*sp*²/*sp*³) component in the C(1s) core level spectra becomes dominant by comparison with unmodified FGS₂ (Figure 5, Figure 6, and Supporting Information Figure SI-2). New contributions appear in the respective C(1s) spectra, examined in further detail below, based on the comparison with the measurements made on the molecular tetrazine Tz5. After functionalization, the single band of the O(1s) spectrum of FGS₂ (Figure 4b) split into a more complex signal containing two or three components in the FGS-Tz materials (Figure 5b, Figure 6b, and Supporting Information Figure SI-2b). One of the added components is higher in energy (533.5 eV) which may correspond to the oxygen now linked to the aromatic tetrazine (C—O—C=).^{30,33}

In the N(1s) core level signal (Figure 5c, Figure 6c, and Supporting Information Figure SI-2c), two components of similar intensity and separated by a significant energy difference (1.3 eV) are systematically observed. It is unexpected that the four nitrogen atoms of the tetrazine units would not be energetically equivalent in the grafted FGS-Tz material. To assign this difference, the XPS spectrum of Tz5 was recorded (Figure 7). This tetrazine derivative was chosen because, due to its high molecular weight, it is stable in the solid phase even under the very low pressure of XPS experiments. As noted previously, XPS on low molecular weight tetrazine derivatives was impractical because the tetrazines readily sublime under low pressure. Figure 7a shows a single peak centered at ca. 401 eV for N(1s) in this molecule, evidence that all the nitrogen atoms in the tetrazine ring are energetically equivalent, as already observed with tetrazine based ligands.³⁴ It was also determined that a chemical oxidative post-treatment of the grafted FGS (FGS-Tz) did not change the shape of the N(1s) signal, excluding the possibility that partially hydrogenated tetrazine rings might exist in the FGS-Tz materials. The two distinct bands in the N(1s) signals of FGS-Tz are thus typical of the Tz-functionalized material and might be due to specific interactions (like hydrogen bonding) between the nitrogen atoms of the tetrazine ring that are closer to the graphene sheets and the functionalities thereon (like carboxylic acids).

As expected, the C(1s) spectrum for Tz5 (Figure 7b) is very simple, revealing three types of carbons consistent with the Tz5 molecular structure: the low energy contribution (284.5 eV) can be unambiguously assigned to the aliphatic carbons of the adamantane core, as they represent 75% of the total amount of carbon atoms. The medium energy signal (286.5 eV) can be assigned to the C—C—O fragment, in agreement with the usual position of ether functional carbons. Finally the high energy band (288.5 eV) comes from the carbon atoms in the tetrazine ring (O—C=N) which are the most oxidized ones and thus lead to the highest energy band. The similar relative proportions of the two latter bands are in agreement with the expected equal atomic ratios of C—C—O and O—C=N in Tz5. From this assignment, one can deduce the probable

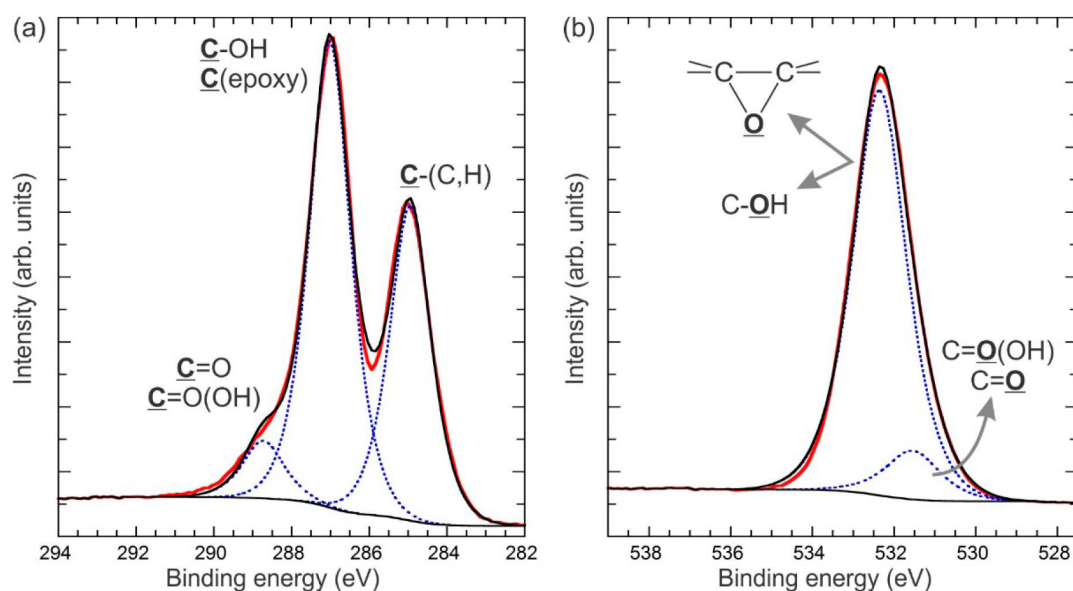


Figure 4. XPS data of unmodified FGS₂: (a) C(1s) and (b) O(1s) core level spectra (red lines) and curve-fitting results (individual assignments are shown as blue dashed lines; the sum of the curves is shown as a black line).

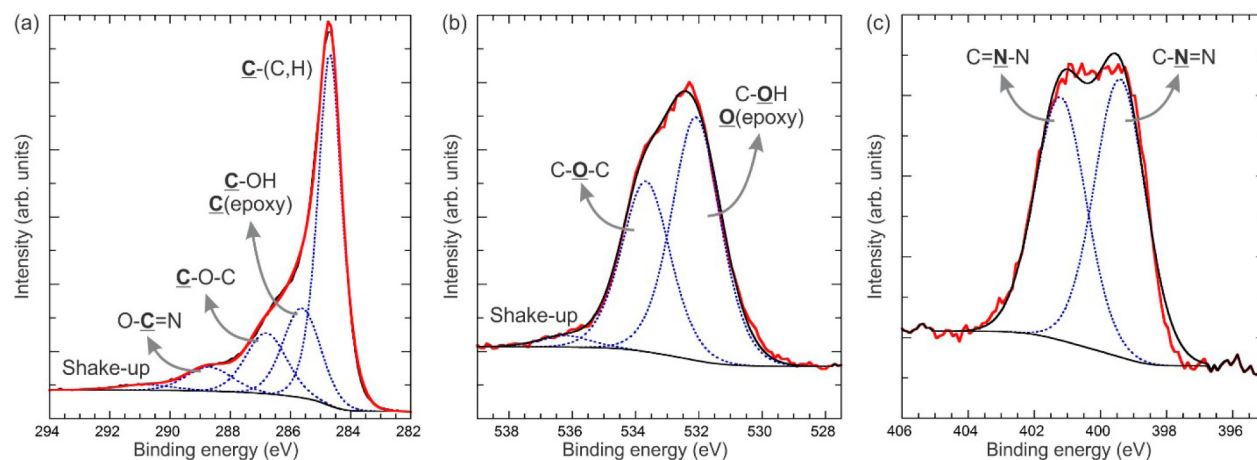


Figure 5. XPS spectra of FGS-Tz3: (a) C(1s), (b) O(1s), and (c) N(1s) core level spectra (red lines) with the results of curve fitting (blue and black lines).

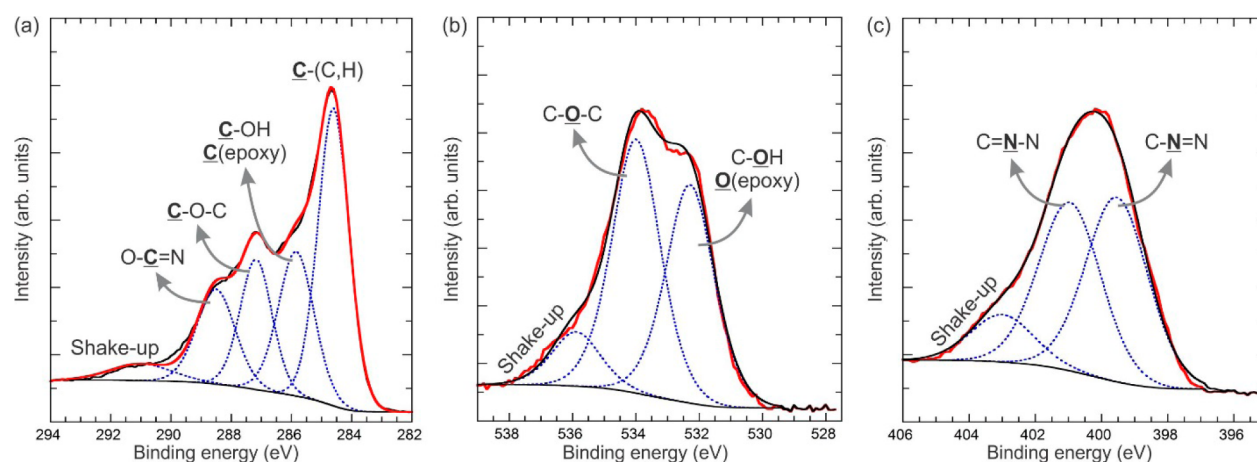


Figure 6. XPS spectra of FGS-Tz4: (a) C(1s), (b) O(1s), and (c) N(1s) core level spectra (red lines) with the results of curve fitting (blue and black lines).

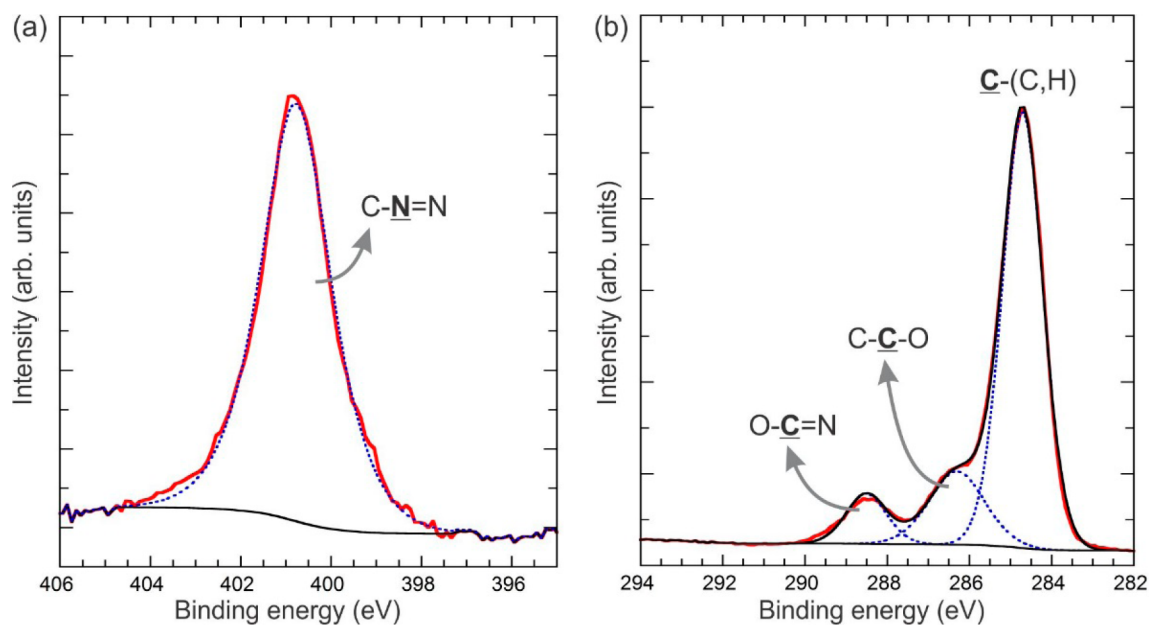


Figure 7. XPS spectra of Tz5: (a) N(1s) and (b) C(1s).

assignments of the C bands in the deconvoluted spectra for the FGS-Tz2–4 compounds. Thus, the highest energy contribution (above 288 eV) mainly involves the carbon atoms of the tetrazine ring (although a contribution from carbonyl and carboxylic functions in FGS₂ is also possible), while the one just below (286.5 eV) corresponds to the carbon atoms linked to oxygen in respectively the butoxy group (FGS-Tz2), the adamantanemethoxy (FGS-Tz3), or the biphenyldioxy linker (FGS-Tz4). Finally the contribution coming from the carbon atoms linked to oxygen in epoxy or unreacted hydroxyl groups of the graphene part of FGS-Tz can be seen at 285.5 eV. This assignment fits well with the increase in the relative intensities of the two more energetic bands (288.5 and 286.5 eV) observed in FGS-Tz4, versus FGS-Tz3, in agreement with the higher amount of grafted tetrazine in the former (see Table 1). Finally, we observe the existence of π -plasmon peaks in the C(1s), N(1s), and O(1s) core level spectra for the FGS-Tz compounds (Figure 5, Figure 6, and Supporting Information Figure SI-2). These π -plasmon peaks, ascribed to π - π^* “shake-up” transitions, are characteristics of aromatic ring structures or unsaturated bonds, and their presence here testifies to the abundance of aromatic/unsaturated tetrazine structures.^{33,35}

The relative amount of grafted tetrazine can be coarsely estimated from the N over O atomic percentages listed in Table 1 for the various functionalized FGS-Tzs. Assuming that all the oxygen content within FGS₂ is in the form of OH groups would lead to the following relationships based on the molecular composition:

$$\%N(\text{FGS}_2\text{-Tz2}) = \frac{4x}{\left(\frac{1}{\%O(\text{FGS}_2)} + 11x\right)} \quad (1)$$

$$\%N(\text{FGS}_2\text{-Tz3}) = \frac{4x}{\left(\frac{1}{\%O(\text{FGS}_2)} + 18x\right)} \quad (2)$$

where %N is the atomic percentage of N in the grafted material, %O(FGS₂) is the atomic percentage of O in the starting material (FGS₂), and x is the proportion of oxygen atoms functionalized by tetrazine in the grafted material. On the basis of the percentages determined from XPS, the grafting atomic ratio can be assessed to respectively 15% in FGS-Tz2 and 6% in FGS-Tz3. As expected, the grafting efficiency is notably lower in FGS-Tz3 due to the bulkiness of the adamantane group.

The same calculation in FGS-Tz4 is complicated by the possibility of single versus double ends (bridging) functionalization, depending on the reactivity of the grafted molecule. The following relations between the nitrogen and chlorine contents and the functionalization ratios can be drawn:

$$\%N(\text{FGS}_2\text{-Tz4}) = \frac{4x + 8y}{\left(\frac{1}{\%O(\text{FGS}_2)} + 13x + 26y\right)} \quad (3)$$

$$\%Cl(\text{FGS}_2\text{-Tz4}) = \frac{y}{\left(\frac{1}{\%O(\text{FGS}_2)} + 13x + 26y\right)} \quad (4)$$

where x is the proportion of oxygen atoms functionalized by bridging units (i.e., those that do not contain chlorine) and y is the proportion of oxygen atoms functionalized by nonbridging tetrazine units (i.e., those terminated by chlorine). The values of x and y can be estimated respectively to 33% and 6%, based upon the chlorine and nitrogen atomic fractions found in FGS-

Tz4. This calculation is based on the fact that any chlorine in FGS-Tz4 comes solely from single ended functionalized tetrazine (e.g., nonbridging molecules), which seems reasonable since the residual chlorine content in FGS-Tz2 and FGS-Tz3 is nearly the same as in FGS₂. Compared to FGS-Tz3, the grafting in FGS-Tz4 is much more efficient, which was expected due to the steric hindrance of the adamantane unit in FGS-Tz3. It is also worth noticing that most of the functionalization involved both sides of the molecule thus effectively leading to bridging FGSs. The rigidity of the molecule makes it unlikely that grafting occurred between two closely spaced hydroxyl groups on the FGS₂. However, FGSs can be folded or bent which may lead to intrasheet grafting.³⁶

When recalculated from the values found for x and y , the oxygen content in FGS-Tz4 is given by

$$\%O(\text{FGS}_2\text{-Tz4}) = \frac{1 + x + y}{\left(\frac{1}{\%O(\text{FGS}_2)} + 13x + 26y\right)} \quad (5)$$

leading to a value of 15%, which is reasonably close to the actual value (11%) determined by XPS.

Thus, we conclude from XPS experiments that tetrazine has been covalently attached to FGS₂ in all the FGS-Tz materials investigated (except with Tz1). Concerning the reaction of Tz4 with FGS₂ we can conclude that the grafting occurs mainly in a form that bridges the FGS₂, with only small amounts of singly bound Tz4 present.

Structural Analysis. Structural differences between pure tetrazines and FGS-Tz compounds as determined by XRD analysis (Figure 8) indicate that all the pure tetrazines precipitate as crystalline powders (Figure 8a) while the FGS-Tz compounds are much less crystalline, except for the FGS-Tz4 compound, the diffraction pattern for which reveals significant crystallization (Figure 8b). For the pure tetrazines, variations in the spacing between the tetrazine rings in the crystals may be indicated by the shift in the low angle diffraction, appearing at 12.6° in Tz1, a strong diffraction peak whose position progressively decreases to less than 5° with increasing substituent size (Figure 8a). The bulky substituent in Tz3 (the methoxyadamantane) and the presence of the biphenyl in Tz4 further complicate the respective diffraction patterns.

The strong diffraction peak at 13.1° for GO in Figure 8b corresponds to a sheet–sheet separation ($d_{002} = 0.68$ nm) between the graphene oxide sheets (basal planes of GO). This GO is first ultrasonicated in propylene carbonate to produce single sheets of graphene oxide (FGS₂). By heating (120 °C for 48 h) FGS₂ in propylene carbonate and the catalyst 2,4,6-trimethylpyridine added after the dispersion process, a reduced FGS_x forms, where x has been reported to range between 6 and 8.²⁷ As shown in Figure 8b, the GO diffraction peak at 13.1° completely disappears and a broad diffraction peak centering around ~ 25° (~ 0.36 nm interlayer spacing) forms for FGS_x. The disappearance of the 13.1° GO peak indicates that the dispersion of single sheets of graphene oxide in propylene carbonate was accomplished. Whereas the formation of the broad peak at ~ 25° suggests the restacking of the FGS_x into a highly disordered state during or after the reduction step. As the interlayer spacing of ~ 0.36 nm of this broad peak corresponds closely to the d_{002} spacing of graphite, along with the reduction, some graphitic patches must be forming in the aggregates. Further, the broad diffraction peak remains after reaction with tetrazines (Figure 8b).²⁷ The diffraction pattern

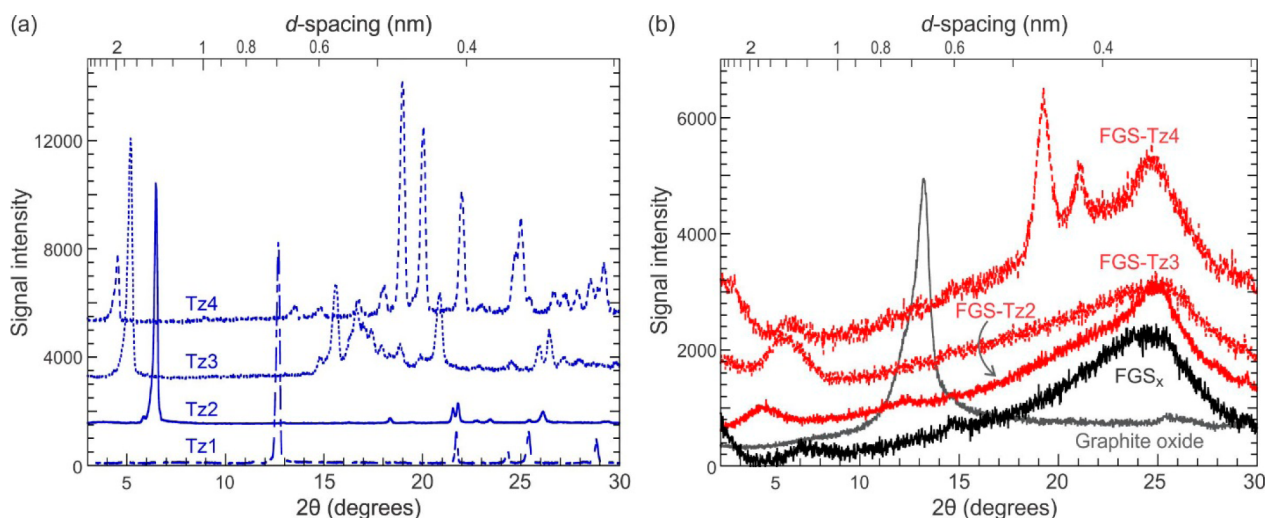


Figure 8. XRD patterns for (a) pure tetrazines after precipitation from solution and (b) the FGS-Tz compounds, GO, and FGS_x.

of the FGS-Tz4 compound exhibits two strong sharp peaks at 19.2° and 21.1° (Figure 8b), near in location to the 19.0°, 20.1°, and 22.0° peaks visible in the diffraction pattern of the pure Tz4 (Figure 8a). However, the absence of any other evidence of free Tz4 in the FGS-Tz4 (also indicated in the CV and XPS discussed above and further confirmed by thermal analysis and FTIR shown in the following) suggests that the diffraction pattern of the FGS-Tz4 is due to induced ordering of the sheets, most probably from the Tz4 acting as a bridging agent to link neighboring sheets.

The stacked morphology of the bridged FGS-Tz4 is also revealed by atomic force microscopy (AFM) imaging when we compare the typical thickness of the thinnest (< 2 nm) FGS_x (Figure 9a) particles with that (~ 1.2 μm) of the FGS-Tz4 (Figure 9b). While the FGS_x particles can be near single sheet thickness, the FGS-Tz4 does not separate into single sheets during sonication and is as thick as > 1.0 μm.

Thermal Analysis. Thermal analysis of the FGS-Tz compounds, unmodified FGS₂ (made by dispersing GO in

propylene carbonate),²⁷ and FGS₁₅ (from the thermal reduction of FGS₂), by thermogravimetry (TG) and differential scanning calorimetry (DSC) provides additional support for the covalent attachment of tetrazines to FGS₂ (Figure 10). Under the slow (5 °C/min) ramp to 325 °C used in this study, the loss of substituted tetrazine from the FGS-Tz compounds appears as a gradual event with no detectable change in the calorimetric properties during heating (Figure 10a), although accompanied by a substantial loss of mass (Figure 10b). A prominent feature of the DSC measurements on unmodified FGS₂ is the strong exotherm observed at ~ 230 °C (Figure 10a) due to the generation of water vapor and carbon dioxide at the onset of rapid thermal reduction.³⁷ This exotherm is not present in thermally reduced FGS (for example, in FGS₁₅) and in the FGS-Tz compounds, indicating that the FGS₂ used to make the FGS-Tz compounds was reduced during the reaction between tetrazine and FGS₂.

The residual masses of the FGS-Tz compounds, after being heated at 325 °C for 1 h (Figure 10a), are in good agreement with the mass of grafted tetrazine indicated by the elemental analysis of the FGS-Tz compounds by XPS (Table 1). A comparison is shown in Table 2. It is important to note that the residual mass measured for FGS-Tz4 assumes some decomposition products are part of the total residual mass, as indicated by the TG of the pure Tz4, whereas Tz2 and Tz3 are assumed to be completely lost during heating. For each FGS-Tz compound, a loss of 4% mass from the FGS was assumed, based on the mass loss exhibited by FGS₁₅ under the same thermal cycle.

In contrast to the grafted tetrazines, the thermal analysis of pure tetrazines indicates high instability (Table 3 and Supporting Information Figure SI-3). The Tz1 precursor readily sublimates from a loosely lidded sample holder during heating, and its thermal properties can only be effectively determined in a sealed sample holder.³⁸ The substituted tetrazines used in this study (Tz2, Tz3, Tz4) are more stable during heating (Supporting Information Figure SI-3), allowing melting points and onset of vaporization to be determined using a loosely lidded sample holder (Table 3) under a nitrogen atmosphere. However, the lower molecular weight (MW) tetrazine derivatives remain quite volatile, with very low residual mass when heated above the vaporization temperature. Only

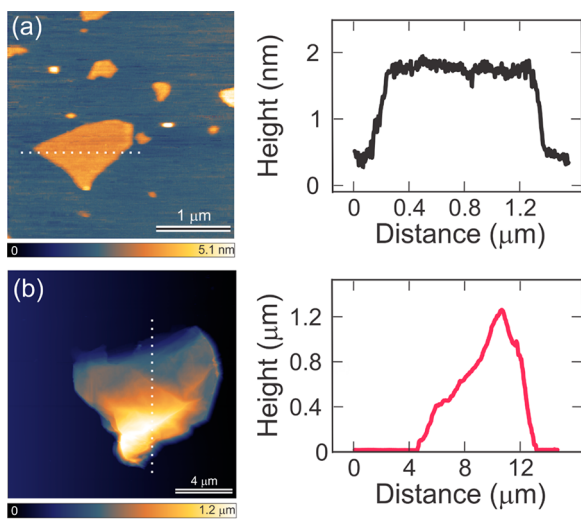


Figure 9. AFM images of (a) FGS_x and (b) FGS-Tz4. The figures on the right of the images show the thickness profile of the particles along white dotted lines.

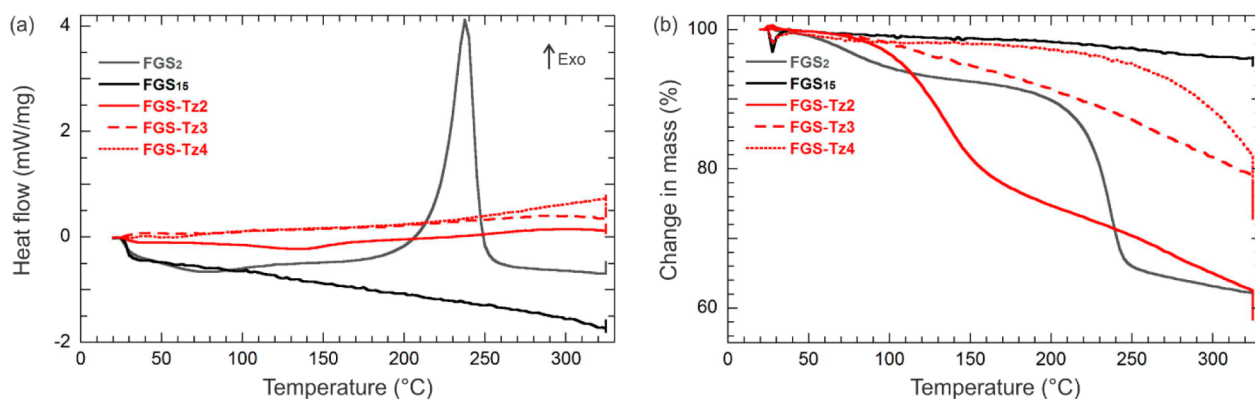


Figure 10. (a) DSC and (b) TG curves for FGS_2 , FGS_{15} , and the FGS-Tz compounds. Samples are heated at $5\text{ }^\circ\text{C}/\text{min}$ under nitrogen to $325\text{ }^\circ\text{C}$ and held at that temperature for 1 h to release any bound tetrazine. The TG curves for FGS_2 and FGS_{15} are shown for comparison. Residual masses following heat treatment are FGS-Tz2 , 58.5% of the original; FGS-Tz3 , 73.6%; FGS-Tz4 , 72.7%; FGS_2 , 60.2%; and FGS_{15} , 95.1%.

Table 2. Tetrazine Content (by mass) in FGS-Tz Compounds

compound	from elemental analysis ^a	from residual mass (TG)
FGS-Tz2	37%	38%
FGS-Tz3	28%	22%
FGS-Tz4	28%	23%

^aAssuming complete loss of Tz2 and Tz3 from the respective compounds but retaining some residual mass from the decomposition of the Tz4 .

Table 3. Phase Transitions in Pure Tetrazines, under Streaming Nitrogen

tetrazine	melting point ($^\circ\text{C}$)	onset of vaporization ($^\circ\text{C}$)	onset of decomposition ($^\circ\text{C}$)	residual mass at $325\text{ }^\circ\text{C}$
Tz1		130 (sublimes)		
Tz2	44	145	n/a	<1%
Tz3	123	226	n/a	<1%
Tz4	246		341	35%

the very high MW substituents (as in Tz4) sufficiently stabilize the inherently energetic tetrazine rings to reach the temperature of decomposition,³⁹ marked by a significant exothermic reaction not seen in the lower MW-substituted tetrazines. The higher MW substituent in Tz4 is not completely consumed, resulting in significant residual mass when the sample is heated under an inert atmosphere.

FTIR. The infrared spectra of the pure tetrazines, FGS-Tz compounds (Figure 11a,b,c), and FGS_2 (Figure 11d) show that tetrazines are closely associated with the FGSs after the reaction. The grafting reactions dry and partially reduce the FGS_2 , the latter also indicated by the loss of the exotherm at $220\text{ }^\circ\text{C}$ in the DSC of the FGS-Tz compounds (Figure 10a). Changes in the chemical composition of the FGS-Tz relative to those of the pure tetrazines and FGS_2 are more apparent when the infrared spectra of the respective materials are compared. The reflectance infrared spectrum of Tz1 (Supporting Information Figure SI-4) exhibits comparatively strong bands at ~ 890 and $\sim 1250\text{ cm}^{-1}$ caused by the presence of C—Cl and fluctuations of the tetrazine ring.⁴⁰ The C—Cl band appears to be shifted to lower frequencies by replacing one chlorine atom with a more electron donating alkoxy group. The C—N ring absorptions also appear to be affected by the presence of the substituent groups. This is apparent in the

spectra of pure tetrazines used in this study (Figure 11) wherein the tetrazine ring is difficult to discern among more intense absorptions in the fingerprint region ($< 1600\text{ cm}^{-1}$) due to the FGS. Conversely, the C—H stretching frequencies of the alkoxy groups in the substituted tetrazines are obvious at higher frequencies and are detectable in the spectra of the FGS-Tz compounds.

As noted previously, Tz1 did not appear to react with the FGS_2 and was instead consumed by side reactions⁴¹ with other components of the reaction mixture. Following the attempted reaction between Tz1 and FGS_2 , the solid was filtered from the reaction mixture, extensively washed, and then dried. No detectable bands attributable to the presence of Tz1 could be seen in the infrared spectrum of the solid, which resembled that of the product from the thermal reduction of FGS_2 . To test the persistence of tetrazines when mechanically mixed with FGS_2 , mixtures were prepared of FGS_2 and the respective tetrazines (at room temperature) to match the compositions shown in Table 2. These mixtures could be washed free of the tetrazine, with little discernible effect on the subsequent infrared spectra of the washed FGS_2 , which, like the unreacted FGS in the $\text{Tz1}/\text{FGS}_2$ mixture, did not exhibit any bands that could be unambiguously assigned to the presence of tetrazines.

The spectral traces of the Tz2 , Tz3 , and Tz4 in the spectra of the corresponding $\text{FGS}_2\text{-Tz}$ compounds are evidence that those tetrazines remained associated with the FGSs following reaction, filtering, and washing (Figure 11a,b,c). The presence of the different tetrazines is revealed in the C—H bands observed between 2800 and 3000 cm^{-1} for FGS-Tz2 (Figure 11a) and FGS-Tz3 (Figure 11b) and in the region $3000\text{--}3100\text{ cm}^{-1}$ for FGS-Tz4 (Figure 11c), the latter a much weaker absorption. The C—H regions are especially useful indicators as there are no detectable bands within these regions of the infrared spectra of unmodified FGS_2 (Figure 11d) and FGSs in general and are well away from the fingerprint region of the infrared spectrum ($< 1600\text{ cm}^{-1}$),⁴² a region complicated by the presence of overlaying features. The presence of the tetrazine unit in the FGS-Tz4 compound is also indicated by the presence of the 4,4'-dihydroxybiphenyl group, seen in the IR spectrum as absorption bands between 1300 and 1500 cm^{-1} . These are related to the phenyl rings, slightly shifted from the positions observed in pure 4,4'-dihydroxybiphenyl.

Moreover, that extensive washing has no apparent effect on the presence of the tetrazines indicates a strong link between the tetrazines and the FGS_2 following reaction.

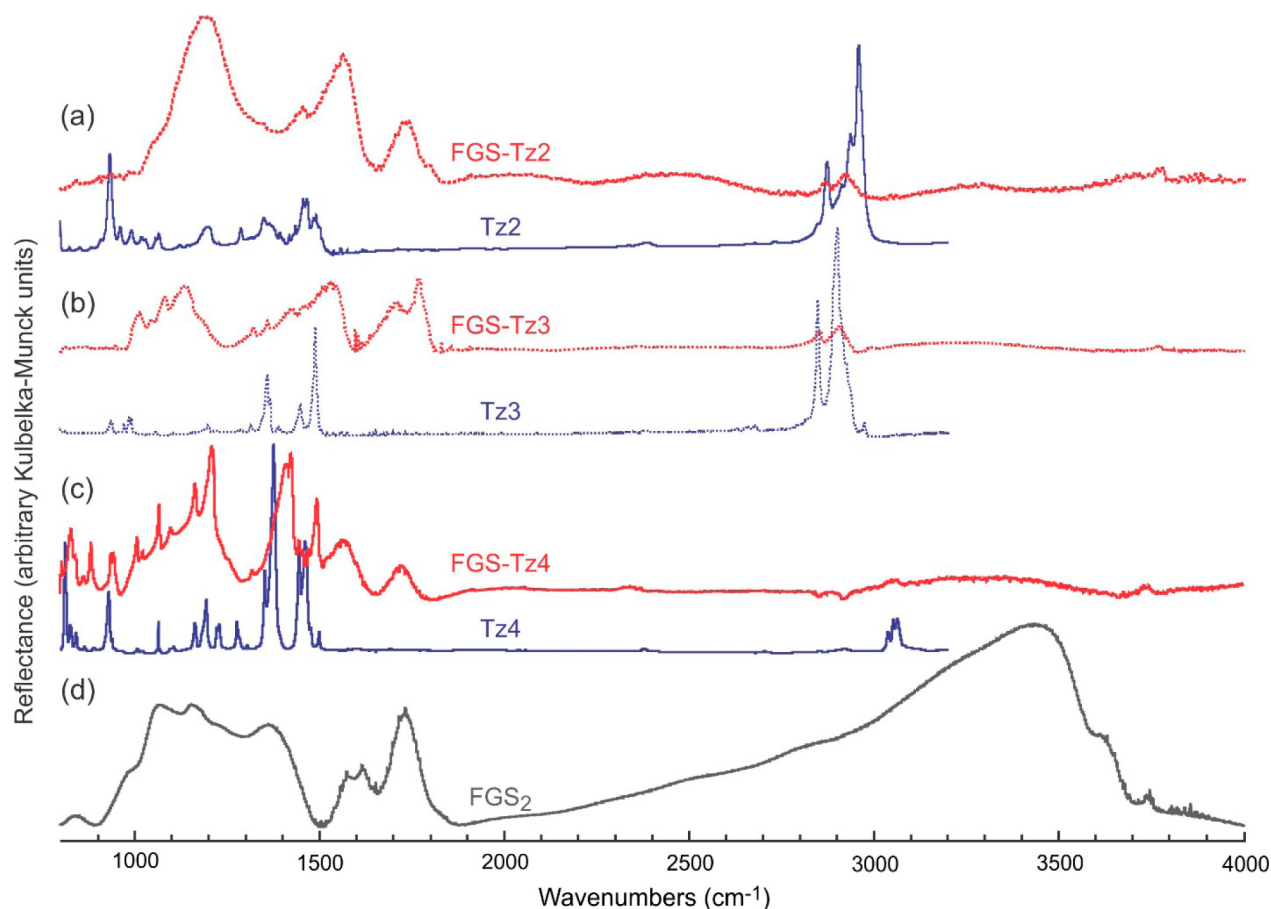


Figure 11. FTIR spectra of (a–c) pure tetrazines and the related FGS-Tz compounds, compared to the spectrum of (d) unmodified (and unreacted) FGS₂. The loss of the large hydroxyl band near 3450 cm⁻¹ indicates that the FGS was dried during the reaction with the chlorotetrazines to form the covalently linked compounds. C–H stretching bands (~2900 cm⁻¹ for Tz2 and Tz3; ~3050 cm⁻¹ for Tz4) indicate the presence of tetrazine in the FGS-Tz compounds, following functionalization and reduction of the FGS₂ by substituted chlorotetrazines.

Due to its intrinsically hydrophilic nature,⁴² the infrared spectrum of FGS₂ is further complicated by the presence of adsorbed water, most apparent as a strong and broad absorbance that peaks near 3450 cm⁻¹, broad enough to distort the reflectance baseline well below 2500 cm⁻¹ (Figure 11d). Sonicating the GO in propylene carbonate to form the FGS₂ suspension did not significantly affect the presence of adsorbed water; the respective IR spectra of the GO and FGS₂ were seen to be very similar. The presence of water broadens absorption bands at lower frequencies through interactions with other oxygen functionalities, for example, in forming hydrogen bonds with hydroxyl groups.⁴³ However, in the case of the FGS-Tz compounds, the amount of physisorbed water (Figure 11a,b,c) is difficult to discern, indicating that the process of grafting tetrazine onto FGS₂ (Scheme 2) also serves to dry the FGS₂ in addition to reducing the FGS₂.

CONCLUSIONS

In this paper it has been demonstrated for the first time that tetrazine derivatives can be covalently attached to graphene oxide through nucleophilic substitution reactions. Cyclic voltammetry, XPS, TA, and FTIR were successively implemented to provide evidence of this covalent grafting. The electrochemical response of the tetrazine units in the grafted materials is significantly shifted from the ones for the starting molecular compounds, due to the sensitivity of the reduction potential of tetrazine moiety to the substitution of a chlorine

atom by an oxygen atom. This response proves the covalent grafting and excludes the possible physisorption of the tetrazine on the graphene oxide. XPS shows a large increase in the nitrogen content and in the C/O of the final materials, while TA and FTIR confirm the reaction efficiency by displaying strong differences between the signatures of the starting compounds compared to the final materials, especially concerning decomposition rate and mass losses. Among the various covalently modified graphenes, one involving a bridging tetrazine unit between graphene sheets displays very specific structural features as demonstrated by XRD and AFM measurements, which opens the way toward new materials with original properties, especially in the framework of composites by allowing an easy insertion of another compound (like an elastomer or a conducting polymer) in this “open” structure. Experiments in this field are in progress to confirm these promising perspectives.

MATERIALS AND METHODS

Synthesis. Reagents were commercially available from Aldrich and used without further purification. Column chromatography was performed with SDS 0.040–0.063 mm silica gel. All compounds were characterized by the usual analytical methods: ¹H, ¹³C NMR spectra were recorded with a JEOL ECS (400 MHz) spectrometer. All chemical shifts are referenced to the solvent peak (*J* values are given in Hz).

The tetrazine derivatives synthesized from **Tz1** and identified as **Tz2**, **Tz3**, **Tz5**, and **Tz6** were prepared as described previously.^{21,44} Our method for synthesizing **Tz4** and then grafting **Tz4** to FGS₂ (FGS-Tz4) is described in the following paragraphs.

Tz4: 4,4'-Dihydroxybiphenyl (931 mg, 5 mmol) is dissolved in 20 mL of CH₂Cl₂. 2,4,6-Trimethylpyridine (1.58 mL, 12 mmol, 2.4 equiv) and **Tz1** (1.81 g, 12 mmol, 2.4 equiv) were added successively, and the mixture was stirred at room temperature under Ar protection. The extent of reaction is checked using TLC; the reaction is determined to be complete when no free tetrazine is found on the chromatographic plate. The final compound was purified by silica gel flash chromatography (eluent: dichloromethane/ethyl acetate (5/5) to dichloromethane/ethyl acetate (2/8)) to give **Tz4** (2.075 g, 63%) as an orange solid. ¹H NMR (400 MHz, CDCl₃) δ (ppm): 7.71 (d, *J* = 8.7 Hz, 4H), 7.38 (d, *J* = 8.7 Hz, 4H). ¹³C NMR (100 MHz, CDCl₃) δ (ppm): 167.7, 165.6, 151.5, 139.0, 129.2, 121.4.

FGS-Tz4: Dry GO powder (60 mg, 1.5 mmol) is bath sonicated in 30 mL of propylene carbonate (PC) (concentration: 2 mg/mL) for 30 min to form a stable suspension of FGS₂ in PC.²⁷ After dispersing the FGS₂, 2,4,6-trimethylpyridine (0.8 mL, 6 mmol) and **Tz4** (124.6 mg, 0.3 mmol) were added successively to the suspension under stirring and Ar protection. The solution was heated at 120 °C for 48 h and then cooled. After cooling to ambient temperature, 30 mL of dichloromethane was added into the suspension and the functionalized graphene and liquid were separated by centrifugation for 30 min; the supernatant was removed, and 30 mL of dichloromethane was again added. The sequence was repeated for 3–4 times, until the supernatant was colorless. The final compound was filtered and rinsed again with dichloromethane, and then dried at room temperature.

FGS-Tz2 and **FGS-Tz3** were prepared using the same procedure. As noted, attempts to synthesize **FGS-Tz1** failed due to a rapid reaction that appeared to involve **Tz1** and PC in the presence of the collidine catalyst.

The GO used to make the FGS₂ suspensions was produced using a modified Hummers method⁴⁵ described previously⁸ and summarized here. In a typical procedure, 3 g of flake graphite (Grade 3061, Asbury Carbons) and 18 g of KMnO₄ were slowly added to 400 mL of a stirred solution composed of 360 mL of H₂SO₄ and 40 mL of H₃PO₄. The oxidation was continued for ~16 h with the temperature of the reaction vessel was held at 50 °C. After cooling, 12 mL of 35 wt % H₂O₂ was added to the stirring suspension and the color of the changed from brown to bright yellow. The suspension was distributed into two 500 mL centrifuge tubes and centrifuged for 15 min at 1800 g (Centra GP8R centrifuge, IEC, Thermo Scientific). The supernatant was discarded, and the material was resuspended in water. This washing procedure was repeated several times, first using 250 mL of 35 wt % HCl (aq) followed by three to four washes using 250 mL of ethanol, until the residual chlorine content was observed to remain stable, as determined by elemental analysis using energy dispersive X-ray spectroscopy (EDS) (INCAx-act, Oxford Instruments, Abingdon, U.K.). The KMnO₄, H₂SO₄, H₃PO₄, HCl (aq), and H₂O₂ used in the synthesis and washing of GO were all high purity and used without modification (Fisher Scientific).

Characterization. For cyclic voltammetry measurements, all FGS and FGS-Tz compounds were redispersed in PC by sonicating for 10 min in a sonication bath. Cyclic voltammetry was performed in a three-electrode cell with a Pt disk as the working electrode, Ag wire as the pseudoreference electrode, and Pt wire as the counter electrode. Measurements were made using a potentiostat (VersaSTAT4, Princeton Applied Research). Propylene carbonate (SDS, HPLC grade) and electrolyte salts (tetrabutylammonium hexafluorophosphate (TBAPF₆) from Fluka, puriss.) were used without further purification. All the tests were performed in TBAPF₆ in PC (0.1 M) with sample concentrations of 0.01 M (FGS, FGS-Tz, or Tz). All solutions and suspensions were deaerated by bubbling with nitrogen for at least 10 min prior to use.

XPS was performed on samples of dry GO and FGS-Tz powders and on samples of FGS₂ or FGS-Tz_s coated on glass slides. Coated glass slides were prepared by sonicating GO (to create a suspension of FGS₂) or the FGS-Tz compounds in acetonitrile for 10 min and then

transferring to glass slides and drying in a fume cupboard at ambient temperature. No differences were observed between the XPS measurements of GO and FGS₂. XPS measurements were carried out at room temperature on an Axis Nova spectrometer (Kratos Analytical) using the Al K α line (1486.6 eV) as the excitation source. Survey spectra were acquired at pass energies of 80 eV. The core level spectra (C(1s), O(1s), Cl(2p), and N(1s)) were acquired with an energy step of 0.1 eV and using a constant pass energy mode of 20 eV, to obtain data in a reasonable experimental time (energy resolution of 0.48 eV). The pressure in the analysis chamber was maintained lower than 10⁻⁷ Pa.

Data analysis was performed using CasaXPS software. The background spectra are considered as Shirley type and curve fitting is carried out with a mixture of Gaussian–Lorentzian functions.⁴⁶ For calibration, the binding energy for the C 1s hydrocarbon peak was set at 284.8 eV. The error in defining the position of peaks is estimated at about 0.1 eV. No surface cleaning, such as using Ar sputtering, was done. We know from experience that carbonaceous atmospheric contamination on material usually occurs, but, in our case, it was thought that ion sputtering might change the chemical composition and cause structural damage.

Powder XRD was performed on dry powders using a Miniflex II (Rigaku Americas, PA, Cu K α radiation). The lowest detectable angle of $2\theta = 5^\circ$ corresponds to an upper limit in the observable *d*-spacing of 1.76 nm.

AFM was performed to determine the topography of the materials using a silicon cantilever in contact mode (Veeco Multimode with Nanoscope IIIa controller). Samples were ultrasonicated in propylene carbonate and then deposited and dried using spin-coating onto a silica substrate.

Thermal analysis was performed using dry samples of pure tetrazines (Tz) and FGS-Tz powders on a simultaneous thermal analyzer (Jupiter 449C STA, Netzsch), combining TG with DSC. All measurements were made on samples contained in Pt–Rh lidded sample containers under nitrogen atmosphere, referenced against an empty Pt–Rh crucible. Sample size was between 3 and 5 mg, and all samples were heated to the maximum temperature from room temperature at a rate of 5 °C/min.

FTIR spectra were collected using a modified diffuse reflectance technique,⁴⁷ in which the sample was deposited from suspension onto a flat mirror surface. As an example of the procedure, to measure the IR adsorption of FGS₂, a few milligrams of GO powder was added to a test tube containing ~2 mL of carbon tetrachloride (Fisher Scientific), shaken, and then sonicated using a hand-held probe sonicator (Branson SLPe, Fisher Scientific) for 5 min. An aliquot was removed from the supernatant using a Pasteur pipet and a few (3–4) drops placed on a circular mirror 1 cm in diameter. The CCl₄ evaporated, leaving a thin layer of the FGS₂ on the surface. The coated mirror was mounted in the sample holder of a diffuse reflectance infrared Fourier transform spectroscopy (DRIFTS) accessory (Collector, Barnes Spectra-Tech) and placed into the sample chamber of an FTIR spectrometer (Nexus 670 FTIR, Thermo Nicolet) equipped with a liquid nitrogen cooled MCT/A detector. Spectra were collected using a slow scan rate (0.16 cm⁻¹ s⁻¹) at 2 cm⁻¹ resolution and signal averaged over 128 scans. Prior to taking spectra, the DRIFTS accessory was aligned for maximum signal throughput using an uncoated mirror, which was also used to provide the background spectrum. Background and sample measurements were taken only after the sample chamber was sufficiently purged using dry nitrogen to reduce the levels of carbon dioxide and water vapor to barely detectable concentrations in the sampling chamber.

■ ASSOCIATED CONTENT

📄 Supporting Information

Additional information for the pure tetrazines and FGS-Tz₂ compound are given in the Supporting Information: (i) the CV for FGS-Tz₃; (ii) the XPS scans for FGS-Tz₂ with curve analysis; (iii) the DSC/TG for the pure tetrazines (see also Table 3); (iv) the FTIR of **Tz1** (3,6-dichloro-*s*-tetrazine); and

(v) TEM images of FGS₂ and FGS-Tz. The Supporting Information is available free of charge on the ACS Publications website at DOI: 10.1021/acs.chemmater.5b00672.

AUTHOR INFORMATION

Corresponding Authors

*(F.M.) E-mail: mioman@ens-cachan.fr.

*(I.A.A.) E-mail: iaksay@princeton.edu.

Present Address

^{||}(M.A.P.) University of Waterloo, Waterloo, Ontario N2L 3G1, Canada

Notes

The authors declare no competing financial interest.

ACKNOWLEDGMENTS

The collaboration between the Ecole Normale Supérieure de Cachan and Princeton University was supported through the Partner University Fund of the French American Cultural Exchange (FACE) through the French Embassy to the United States. The work at Princeton was also partially supported by a Multidisciplinary University Research Initiative (MURI) through the Air Force Office of Scientific Research (AFOSR) under grant AFOSR FA9550-13-1-0004.

REFERENCES

(1) Kucinskis, G.; Bajars, G.; Kleperis, J. Graphene in lithium ion battery cathode materials: A review. *J. Power Sources* **2013**, *240*, 66–79.

(2) Chen, D.; Zhang, H.; Liu, Y.; Li, J. Graphene and its derivatives for the development of solar cells, photoelectrochemical, and photocatalytic applications. *Energy Environ. Sci.* **2013**, *6*, 1362–1387.

(3) Sun, D.-M.; Liu, C.; Ren, W.-C.; Cheng, H.-M. A review of carbon nanotube- and graphene-based flexible thin-film transistors. *Small* **2013**, *9*, 1188–1205.

(4) Ramanathan, T.; Abdala, A. A.; Stankovich, S.; Dikin, D. A.; Herrera-Alonso, M.; Piner, R. D.; Adamson, D. H.; Schniepp, H. C.; Chen, X.; Ruoff, R. S.; et al. Functionalized graphene sheets for polymer nanocomposites. *Nat. Nanotechnol.* **2008**, *3*, 327–331.

(5) Mao, H. Y.; Laurent, S.; Chen, W.; Akhavan, O.; Imani, M.; Ashkarran, A. A.; Mahmoudi, M. Graphene: Promises, facts, opportunities, and challenges in nanomedicine. *Chem. Rev.* **2013**, *113*, 3407–3424.

(6) Yan, L.; Punckt, C.; Aksay, I. A.; Mertin, W.; Bacher, G. Local voltage drop in a single functionalized graphene sheet characterized by kelvin probe force microscopy. *Nano Lett.* **2011**, *11*, 3543–3549.

(7) Punckt, C.; Muckel, F.; Wolff, S.; Aksay, I. A.; Chavarin, C. A.; Bacher, G.; Mertin, W. The effect of degree of reduction on the electrical properties of functionalized graphene sheets. *Appl. Phys. Lett.* **2013**, *102*, 023114-5.

(8) Pope, M. A.; Korkut, S.; Punckt, C.; Aksay, I. A. Supercapacitor electrodes produced through evaporative consolidation of graphene oxide-water-ionic liquid gels. *J. Electrochem. Soc.* **2013**, *160*, A1653–A1660.

(9) Chen, D.; Feng, H.; Li, J. Graphene oxide: Preparation, functionalization, and electrochemical applications. *Chem. Rev.* **2012**, *112*, 6027–6053.

(10) Wang, D.; Kou, R.; Choi, D.; Yang, Z.; Nie, Z.; Li, J.; Saraf, L. V.; Hu, D.; Zhang, J.; Graff, G. L.; et al. Ternary self-assembly of ordered metal oxide–graphene nanocomposites for electrochemical energy storage. *ACS Nano* **2010**, *4*, 1587–1595.

(11) Georgakilas, V.; Otyepka, M.; Bourlinos, A. B.; Chandra, V.; Kim, N.; Kemp, K. C.; Hobza, P.; Zboril, R.; Kim, K. S. Functionalization of graphene: covalent and non-covalent approaches, derivatives and applications. *Chem. Rev.* **2012**, *112*, 6156–6214.

(12) Shen, J.; Shi, M.; Yan, B.; Ma, H.; Li, N.; Hu, Y.; Ye, M. Covalent attaching protein to graphene oxide via diimide-activated amidation. *Colloids Surf., B* **2010**, *81*, 434–438.

(13) Lomeda, J. R.; Doyle, C. D.; Kosynkin, D. V.; Hwang, W. F.; Tour, J. M. Diazonium functionalization of surfactant-wrapped chemically converted graphene sheets. *J. Am. Chem. Soc.* **2008**, *130*, 16201–16206.

(14) Sun, Z. Z.; Kohama, S.; Zhang, Z. X.; Lomeda, J. R.; Tour, J. M. Soluble graphene through edge-selective functionalization. *Nano Res.* **2010**, *3*, 117–125.

(15) Karousis, N.; Sandanayaka, A. S. D.; Hasobe, T.; Economopoulos, S. P.; Sarantopoulou, E.; Tagmatarchis, N. Graphene oxide with covalently linked porphyrin antennae: Synthesis, characterization and photophysical properties. *J. Mater. Sci.* **2011**, *21*, 109–117.

(16) Xu, Y. F.; Liu, Z. B.; Zhang, X. L.; Wang, Y.; Tian, J. G.; Huang, Y.; Ma, Y. F.; Zhang, X. Y.; Chen, Y. S. A graphene hybrid material covalently functionalized with porphyrin: Synthesis and optical limiting property. *Adv. Mater.* **2009**, *21*, 1275–1279.

(17) Xu, H.; Deng, Y.; Shi, Z.; Qian, Y.; Meng, Y.; Chen, G. Graphene-encapsulated sulfur (GES) composites with a core-shell structure as superior cathode materials for lithium-sulfur batteries. *J. Mater. Chem. A* **2013**, *1*, 15142–15149.

(18) Herrera-Alonso, M.; Abdala, A. A.; McAllister, M. J.; Aksay, I. A.; Prud'homme, R. K. Intercalation and stitching of graphite oxide with diaminoalkanes. *Langmuir* **2007**, *23*, 10644–10649.

(19) Abdullah, N.; Hatano, K.; Ando, D.; Kubo, M.; Koshio, A.; Kokai, F. Solubilization of graphene flakes through covalent modification with well-defined azido-terminated poly(epsilon-caprolactone). *J. Appl. Polym. Sci.* **2015**, *132*, 41569.

(20) Englert, J. M.; Dotzer, C.; Yang, G.; Schmid, M.; Papp, C.; Gottfried, J. M.; Steinrück, H.-P.; Spiecker, E.; Hauke, F.; Hirsch, A. Covalent bulk functionalization of graphene. *Nat. Chem.* **2011**, *3*, 279–286.

(21) Clavier, G.; Audebert, P. *s*-Tetrazines as building blocks for new functional molecules and molecular materials. *Chem. Rev.* **2010**, *110*, 3299–3314.

(22) Audebert, P.; Miomandre, F.; Clavier, G.; Vernieres, M. C.; Badré, S.; Méallet-Renault, R. Synthesis and properties of new tetrazines substituted by heteroatoms: Towards the world's smallest organic fluorophores. *Chem.-Eur. J.* **2005**, *11*, 5667–5673.

(23) Sarkar, S.; Bekyarova, E.; Haddon, R. C. Chemistry at the Dirac Point: Diels-Alder Reactivity of Graphene. *Acc. Chem. Res.* **2012**, *45*, 673–682.

(24) Malinge, J.; Allain, C.; Galmiche, L.; Miomandre, F.; Audebert, P. Preparation, photophysical, electrochemical, and sensing properties of luminescent tetrazine-doped silica nanoparticles. *Chem. Mater.* **2011**, *23*, 4599–4605.

(25) Malinge, J.; Allain, C.; Brosseau, A.; Audebert, P. White fluorescence from core-shell silica nanoparticles. *Angew. Chem., Int. Ed.* **2012**, *51*, 8534–8537.

(26) Hayden, H.; Gun'ko, Y. K.; Perova, T. S. Chemical modification of multi-walled carbon nanotubes using a tetrazine derivative. *Chem. Phys. Lett.* **2007**, *435*, 84–89.

(27) Zhu, Y.; Stoller, M. D.; Cai, W.; Velamakanni, A.; Piner, R. D.; Chen, D.; Ruoff, R. S. Exfoliation of graphite oxide in propylene carbonate and thermal reduction of the resulting graphene oxide platelets. *ACS Nano* **2010**, *4*, 1227–1233.

(28) Gong, Y.-H.; Audebert, P.; Clavier, G.; Miomandre, F.; Tang, J.; Badré, S.; Méallet-Renault, R.; Naidus, E. Preparation and physicochemical studies of new multiple rings *s*-tetrazines. *New J. Chem.* **2008**, *32*, 1235–1242.

(29) Lerf, A.; He, H. Y.; Forster, M.; Klinowski, J. Structure of graphite oxide revisited. *J. Phys. Chem. B* **1998**, *102*, 4477–4482.

(30) Briggs, D.; Beamson, G. *High Resolution XPS of Organic Polymers*; John Wiley & Sons Inc.: 1992.

(31) Jin, M.; Jeong, H. K.; Kim, T. H.; So, K. P.; Cui, Y.; Yu, W. J.; Ra, E. J.; Lee, Y. H. Synthesis and systematic characterization of functionalized graphene sheets generated by thermal exfoliation at low temperature. *J. Phys. D: Appl. Phys.* **2010**, 275402.

(32) Bai, H.; Xu, Y.; Zhao, L.; Li, C.; Shi, G. Non-covalent functionalization of graphene sheets by sulfonated polyaniline. *Chem. Commun.* **2009**, *45*, 1667–1669.

(33) Wang, H.; Hao, Q.; Yang, X.; Lu, L.; Wang, X. Effect of graphene oxide on the properties of its composite with polyaniline. *ACS Appl. Mater. Interfaces* **2010**, *2*, 821–828.

(34) Varughese, B.; Chellamma, S.; Lieberman, M. XPS study of self-assembly of ruthenium dimers $[(\text{acac})_2\text{Ru}]_2\text{bptz}]^{0+}$ on hydrophobic and hydrophilic SAMs. *Langmuir* **2002**, *18*, 7964–7970.

(35) Biniak, S.; Szymański, G.; Siedlewski, J.; Świątkowski, A. The characterization of activated carbons with oxygen and nitrogen surface groups. *Carbon* **1997**, *35*, 1799–1810.

(36) Schniepp, H. C.; Kudin, K. N.; Li, J.-L.; Prud'homme, R. K.; Car, R.; Saville, D. A.; Aksay, I. A. Bending properties of single functionalized graphene sheets probed by atomic force microscopy. *ACS Nano* **2008**, *2*, 2577–2584.

(37) McAllister, M. J.; Li, J. L.; Adamson, D. H.; Schniepp, H. C.; Abdala, A. A.; Liu, J.; Herrera-Alonso, M.; Milius, D. L.; Car, R.; Prud'homme, R. K.; et al. Single sheet functionalized graphene by oxidation and thermal expansion of graphite. *Chem. Mater.* **2007**, *19*, 4396–4404.

(38) Oxley, J. C.; Smith, J. L.; Zhang, J. Decomposition pathways of some 3,6-substituted *s*-tetrazines. *J. Phys. Chem. A* **2000**, *104*, 6764–6777.

(39) Bhattacharya, A.; Guo, Y. Q.; Bernstein, E. R. Unimolecular decomposition of tetrazine-N-oxide based high nitrogen content energetic materials from excited electronic states. *J. Chem. Phys.* **2009**, *131*, 194304.

(40) Spencer, G. H.; Cross, P. C.; Wiberg, K. B. *s*-Tetrazine. 2. Infrared Spectra. *J. Chem. Phys.* **1961**, *35*, 1939–1945.

(41) Lang, W. Multifunctional nanocatalysts for fuel combustion: Modification of functionalized graphene sheets with tetrazine molecules. Senior Thesis, Princeton University, 2013.

(42) Dimiev, A.; Kosynkin, D. V.; Alemany, L. B.; Chaguine, P.; Tour, J. M. Pristine graphite oxide. *J. Am. Chem. Soc.* **2012**, *134*, 2815–2822.

(43) Szabó, T.; Berkesi, O.; Dékány, I. DRIFT study of deuterium-exchanged graphite oxide. *Carbon* **2005**, *43*, 3186–3189.

(44) Gong, Y.-H.; Miomandre, F.; Méallet-Renault, R.; Badré, S.; Galmiche, L.; Tang, J.; Audebert, P.; Clavier, G. Synthesis and physical chemistry of *s*-tetrazines: Which ones are fluorescent and why? *Eur. J. Org. Chem.* **2009**, 6121–6128.

(45) Marcano, D. C.; Kosynkin, D. V.; Berlin, J. M.; Sinitskii, A.; Sun, Z. Z.; Slesarev, A.; Alemany, L. B.; Lu, W.; Tour, J. M. Improved synthesis of graphene oxide. *ACS Nano* **2010**, *4*, 4806–4814.

(46) Berresheim, K.; Mattern-Klosson, M.; Wilmers, M. A standard form of spectra for quantitative ESCA-analysis. *Fresenius' J. Anal. Chem.* **1991**, *341*, 121–124.

(47) Venter, J. J.; Vannice, M. A. A diffuse reflectance FTIR spectroscopic (DRIFTS) investigation of carbon-supported metal carbonyl clusters. *J. Am. Chem. Soc.* **1987**, *109*, 6204–6205.